JOURNAL OF Materials CHEMISTRY

Structural modelling of Eu^{3+}-based siloxane–poly(oxyethylene) nanohybrids

K. Dahmouche,[a] L. D. Carlos,*[b] V. de Zea Bermudez,[c] R. A. Sá Ferreira,[b] C. V. Santilli[a] and A. F. Craievich[d]

[a]*Instituto de Química/UNESP, C.P. 355, 14800-900 Araraquara-SP, Brasil*
[b]*Departamento de Física, Universidade de Aveiro, 3810-193 Aveiro, Portugal. E-mail: lcarlos@fis.ua.pt*
[c]*Departamento de Química, Universidade de Trás-os Montes e Alto Douro, Quinta de Prados, Apartado 202, 5001 Vila Real Codex, Portugal*
[d]*Instituto de Física/USP, São Paulo-SP, Brasil*

Received 1st June 2001, Accepted 28th September 2001
First published as an Advance Article on the web 7th November 2001

The modelling of the local structure of sol–gel derived Eu^{3+}-based organic/inorganic hybrids is reported, based on Small-Angle X-ray Scattering (SAXS), photoluminescence and mid-infrared spectroscopy. The hybrid matrix of these organically modified silicates, classed as di-ureasils and termed U(2000) and U(600), is formed by poly(oxyethylene) (POE) chains of variable length grafted to siloxane domains by means of urea cross-linkages. Europium triflate, $Eu(CF_3SO_3)_3$, was incorporated in the two di-ureasil matrices with compositions $400 \geqslant n \geqslant 10$, n is the molar ratio of ether oxygens per Eu^{3+}. The SAXS data for undoped hybrids ($n=\infty$) show the presence of a well-defined peak attributed to the existence of a liquid-like spatial correlation of siloxane rich domains embedded in the polymer matrix and located at the ends of the organic segments. The obtained siloxane particle gyration radius Rg_1 is around 5 Å (error within 10%), whereas the interparticle distance d is 25 ± 2 Å and 40 ± 2 Å, for U(600) and U(2000), respectively. For the Eu^{3+}-based nanocomposites the formation of a two-level hierarchical local structure is discerned. The primary level is constituted by strongly spatially correlated siloxane particles of gyration radius Rg_1 (4–6 and 3–8 Å, errors within 5%, for $U(600)_nEu(CF_3SO_3)_3$, $200 \geqslant n \geqslant 40$, and $U(2000)_nEu(CF_3SO_3)_3$, $400 \geqslant n \geqslant 40$, respectively) forming large clusters of gyration radius Rg_2 ($\approx 75 \pm 10$ Å). The local coordination of Eu^{3+} in both di-ureasil series is described combining the SAXS, photoluminescence and mid-infrared results. In the di-ureasils containing long polymer chains, $U(2000)_nEu(CF_3SO_3)_3$, the cations interact exclusively with the carbonyl oxygens atoms of the urea bridges at the siloxane–POE interface. In the hybrids containing shorter chains, $U(600)_nEu(CF_3SO_3)_3$ with n ranging from 200 to 60, the Eu^{3+} ions interact solely with the ether-type oxygens of the polymer chains. Nevertheless, in this latter family of hybrids a distinct Eu^{3+} local site environment involving the urea cross-linkages is detected when the europium content is increased up to $n=40$.

Introduction

In recent years, the sol–gel method has successfully led to the production of a significant number of novel organic/inorganic frameworks with tuneable design and suitable properties.[1–4] The combination of the appropriate processing conditions with the adequate choice of the organic and inorganic components dictates the morphology, molecular structure and features of the xerogels. The intense activity in this domain of research is due to the extraordinary implications that derive from the possibility of tailoring multi-functional advanced compounds by mixing, at the nanosize level, in a single material organic and inorganic components.[1–4] The synergy of that combination and the particular role of the inner organic/inorganic interfaces enlarge the scope of application of nanohybrid materials in areas such as electrochemistry, biology, mechanics, ceramics, electronics and optics.[2–6]

The hybrid concept seems to be particularly well adapted for the production of photonic materials with potential optical and electro-optical applications, such as, for instance, hybrid layers for optical data storage, optical waveguides, stable non-linear optical materials, sensors or gel-glass dispersed liquid crystals, electrochromic hybrids for smart windows, solid state lasers, and screen displays.[2–6] In the quest for the development of technological applications using hybrid materials two main strategies have been essentially adopted. The first one involves the synthesis of stable and efficient white light photoluminescent organic/inorganic hybrids lacking activator metal ions.[7–13] These hybrids show a potential technological relevance as full colour displays, which is unquestionably one of the main challenging tasks for the next generation of flat panel display systems and lighting technologies. The second one has been focused on the development of suitable hybrid cages capable of encapsulating luminescent centres (organic dyes and lanthanide ions), protecting them from quenching processes. The host structure should also lead itself to an enhancement of light absorption through the so-called antenna effect.[14] These lanthanide-based hybrid hosts combine the mechanical resistance, thermal stability, optical quality and amorphous character of the siliceous skeleton with the optical features of the active luminescent species (namely the high chromaticity and long-excited lifetime characteristic of the lanthanide ions), and, therefore, they have attracted substantial interest.[15–18]

Among the various organic/inorganic hosts that have been proposed in the last years, the family of extremely versatile compounds classed as di-ureasils, in which polyether-based chains of variable length are grafted on both ends to a siliceous backbone through urea functionalities, is noteworthy.[9–13,19–27]

The incorporation of Eu^{3+} [9,20–26] or Tb^{3+} [27] ions into the di-ureasils has led to the synthesis of sol–gel derived

multi-wavelength phosphors where an intrinsic hybrid's network green-blue band is superposed on the typical intra-4f Eu^{3+} and Tb^{3+} lines. As the relative intensity between the broad band and these lines depends on the excitation wavelength and on the amount of lanthanide ions incorporated,[9,23–26] the colour emitted by the doped di-ureasils may be readily tuned across the CIE (Commission Internationale d'Eclairage) chromaticity diagram.[25]

The Small-Angle X-ray Scattering (SAXS) technique is particularly adequate for studying the structure of hybrid materials because of their disordered nature and of the contrast of electronic densities between the organic and inorganic phases.[28–34] In recent works,[11,28,34] the structure of the undoped di-ureasil xerogels has been investigated by SAXS. According to the structural model proposed for these systems,[11,28,34] the hybrids are constituted by dispersed and spatially correlated siloxane clusters, chemically cross-linked to the ends of the polymeric chains. However, the effects of lanthanide doping on the structure of these nanocomposites are not known, making difficult the optimisation of the emission properties of the resulting multi-wavelength hybrid phosphors. A more detailed picture of the local structure of these di-ureasil hybrids is thus essential even though we possess arguments indicating that the local structure of both organic and inorganic phases determines the detected emission features. We can mention, for instance, that the energy range of the broader band emission depends on the siloxane domain sizes,[11–13] on the excitation wavelength, and on the amount of Eu^{3+} ions incorporated.[9,23–26]

In the present study, we use SAXS, photoluminescence, and mid-infrared spectroscopy to analyse urea cross-linked siloxane–poly(ethylene oxide) (POE) hybrids in which different amounts of europium triflate, $Eu(CF_3SO_3)_3$, are incorporated. This work aims to establish a structural local model for the di-ureasil nanocomposites and determine the structural modifications produced as the Eu^{3+} content and the length of the polymer chains are varied. The ultimate goal of the present study is to relate these changes to the overall luminescence features of the hybrids.

Experimental

Sample preparation

The synthesis of the Eu^{3+}-based xerogels has already been described in detail elsewhere.[9,20,22] The covalent bonds between the alkoxysilane precursor (3-isocyanatopropyltriethoxysilane, ICPTES, Fluka) and the oligopolyoxyethylene segment are formed by reacting the isocyanate group of the former compound with the terminal amine groups of doubly functional amines (chemically α,ω-diaminepoly(oxyethylene-co-oxypropylene) and commercially Jeffamine-ED®, Fluka) in tetrahydrofuran. Two Jeffamines with two distinct POE average molecular weights (600 and 2000 g mol^{-1}, corresponding to approximately 8.5 and 40.5 OCH_2CH_2 repeat units, respectively) were used. Urea cross-linked organic–inorganic precursors were thus obtained.[22] $Eu(CF_3SO_3)_3$ (Aldrich) was incorporated in the sol–gel step by dissolving it in ethanol and water (molar proportion 1 ICPTES : 4 CH_3CH_2OH : 1.5H_2O). Both solvents are used to start the hydrolysis and condensation reactions, which lead to the formation of monolithic gels. The doped siloxane–POE hybrids have been designated $U(600)_n Eu(CF_3SO_3)_3$ and $U(2000)_n Eu(CF_3SO_3)_3$, where n = O/Eu represents the number of ether-type oxygens of POE per Eu^{3+} cation. Samples with $n=\infty$, 400, 200, 100, 80, 60, and 40 were prepared. For the sake of clarity for $U(600)_{400}Eu(CF_3SO_3)_3$ the Eu^{3+} mass concentration (relatively to the hybrid's total mass) is 0.3%, corresponding to 94 Si atoms (or urea groups) per Eu^{3+} incorporated, (0.6% and 20, respectively, for $U(2000)_{400}Eu(CF_3SO_3)_3$). In the case of the samples with $n=40$ the Eu^{3+} mass concentration is 2.6% and 5.0%, for the U(600) and U(2000) nanohybrids, respectively (9 and 2 urea groups per Eu^{3+} ion). A salt-rich $U(600)_{10}Eu(CF_3SO_3)_3$ nanocomposite (Eu^{3+} mass concentration of 12.5%, 0.5 urea groups per Eu^{3+} ion) was also synthesised as its infrared analysis enabled us to better illustrate the changes that occur in the Eu^{3+}-first coordination shell when the europium content is increased up to $n=40$.

Techniques

X-Ray scattering measurements were performed using the synchrotron SAXS beamline of the National Synchrotron Light Laboratory (LNLS, Campinas, Brazil). The SAXS beamline is equipped with an asymmetrically cut and bent silicon (111) monochromator that yields a monochromatic ($\lambda=$ 1.608 Å) and horizontally focused beam. A vertical position-sensitive X-ray detector and a multichannel analyser were used to record the SAXS intensity, $I(q)$, as a function of the modulus of the scattering vector q, $q=(4\pi/\lambda)\sin(\varepsilon/2)$, ε being the scattering angle. Each SAXS spectrum corresponds to a data collection time of 300 s. Due to the small size of the incident beam cross section at the detection plane no mathematical desmearing of the experimental SAXS intensity function was needed.[35] The relative error for SAXS intensity, $\Delta I(q)/I(q)$, was determined as the statistical error in the number of photons N collected during 300 s, $\Delta I(q)/I(q)=2/\sqrt{N}$. This statistical error was only significant for low scattering intensities, which are usually found in the high q-range ($q>0.4$ $Å^{-1}$). The parasitic scattering from air, slits and windows was subtracted from the total intensity. This scattering intensity was much weaker than that produced by the samples except over the asymptotic high q range.

The room temperature photoluminescence spectra were recorded under continuous Xe arc lamp (450 W) excitation with a SPEX Fluorolog F212I spectrofluorimeter coupled to a Hamamatsu R928 photomultiplier. All the spectra were corrected for optics and detection spectral response. At 14 K, a 0.25 m excitation KRATOS GM-252 monochromator and a 1 m 1704 SPEX Czerny-Turner spectrometer were used. The time-resolved spectra (14 K) were recorded using a pulsed Xe arc lamp (5 mJ $pulse^{-1}$, 3 μs bandwidth) and a phosphorimeter (SPEX 1934 C).

Mid-infrared spectra were acquired at room temperature using a Unicam FT-IR system. The spectra were collected over the range 4000–400 cm^{-1} by averaging 60 scans at a maximum resolution of 1 cm^{-1}. Solid samples (2 mg) were finely ground and analysed by dispersing them in approximately 175 mg of dried spectroscopic grade potassium bromide (KBr, Merck) by the pressed-disc technique. Prior to recording the spectra under ambient conditions the discs were vacuum-dried at about 323 K for more than two weeks in order to reduce the levels of adsorbed water. In order to evaluate complex band envelopes and to identify underlying component bands of the spectra, an iterative least-squares curve-fitting procedure was used extensively throughout this study.

Method of SAXS analysis

Dilute systems of isolated particles. The simplest structural model for a set of colloidal isolated particles embedded in a homogeneous matrix is a "two electronic density" model composed of spherical objects spatially distributed at random. For this model SAXS intensity is defined by the square of the known form factor, $\varphi(q)$, of the sphere.[35] For a dilute system of particles, the scattering intensity has asymptotic behaviour at low q given by the Guinier law, $I(q)=I(0)\exp(-q^2Rg^2/3)$, where Rg is the radius of gyration of the particles.[35] In the case of spherical particles, $Rg=(3/5)^{1/2}R$, R being the particle radius. At high q, $\varphi(q)$ exhibits oscillatory behaviour. In real materials the particles are often not perfectly spherical and/or

do not all have exactly the same radius. In these cases the oscillations at high q are smeared out. Beaucage *et al.*[31] have proposed an equation for the intensity scattered by non-interacting nearly spherical particles with approximately the same size which exhibit both Guinier and Porod[36] asymptotic behaviour. This equation is given by:

$$I(q) = G \exp(-q^2Rg^2/3) + B[\mathrm{erf}(qRg/6)^3)/q]^4 \quad (1)$$

The first term is a Gaussian decay in scattering intensity at small q, which depends on the particle radius of gyration Rg (Guinier law). In the high q range, Porod's law[36] applies:

$$I(q) = B/q^4 \quad (2)$$

where

$$B = 2\pi(\rho_p - \rho_m)^2 \, S \quad (3)$$

S is the interface area between the two phases per unit volume and ρ_p and ρ_m are the average electron densities of the particles and the matrix, respectively.[36] The constant G is given by:[31]

$$G = NV^2_0 \, (\rho_p - \rho_m)^2 \quad (4)$$

where N is the number of particles per unit volume and V_0 the particle volume. From eqn. (3) and (4) we can deduce the relation between B and G in the case of spherical particles, $B/G = 81/(50Rg^4)$.

The proposed two-phase model (siloxane spheres embedded in a homogeneous polymeric matrix) can safely be applied provided the siloxane particles are isolated and compact, have a nearly isodiametric shape and all have a similar size. The consistency of the model has to be verified by an analysis of the quality of the agreement between the theoretical and experimental SAXS curves. It should be pointed out that a similar multiple scale structure model based on identical spherical particles embedded in a homogeneous matrix has been successfully applied by Beaucage *et al.*[31] to experimental SAXS data of similar siloxane–polymer nanocomposites. Obviously, unacceptable fittings of the theoretical curves to experimental data would indicate that the real structure of the hybrids deviates significantly from the proposed model.

Concentrated systems of particles. The SAXS function, $I(q)$, corresponding to an isotropic structure model consisting of a dense set of spherical colloidal particles of approximately the same size with short range spatial correlation embedded in a homogeneous matrix, is given by:[31,36]

$$I(q) = NP(q) \, S(q) \quad (5)$$

$P(q)$ is a function only of the form factor of the particle—whose q-dependence is described by eqn. (1)—and $S(q)$ is the structure function accounting for short range spatial correlations between them. Beaucage *et al.*[31] proposed the following semi-empirical function for $S(q)$ based on Born–Green theory:

$$S(q) = 1/1 + k\theta(q) \quad (6)$$

where $\theta(q)$, the form factor for structural correlation occurring between particles, is given by:

$$\theta(q) = 3[\sin(qd) - qd\cos(qd)]/(qd)^3 \quad (7)$$

where d is the average interparticle distance and k is a packing factor equal to 8 times the ratio of the average "hard-core" volume of a sphere, V_0, per the average volume available to a sphere, V_1. Eqn. (5), with $P(q)$ and $S(q)$ defined by eqn. (1) and (6), respectively, applies to systems composed of spheres consisting of a hard core and an external shell with an average radius $R' = d/2$. This model seems to be suited, as a first approximation, to our siloxane particles (the hard core) surrounded by soft (polymeric) shells.

Two-level structure. The total scattering intensity produced by a two-level structure can be described, under certain assumptions,[31] as additive contributions from the individual levels. Small volumes (clusters or islands), each of them composed of a dense set of particles, embedded in a low-density matrix give a contribution to the total intensity at very small q. This contribution to SAXS intensity from the second level could also be described by eqn. (1) but, due to the limitation imposed by the minimum accessible q-value, only the asymptotic Porod range can be observed.

Results

SAXS

The SAXS spectra of $U(600)_nEu(CF_3SO_3)_3$ ($200 \geqslant n \geqslant 40$) and $U(2000)_nEu(CF_3SO_3)_3$ ($400 \geqslant n \geqslant 40$) samples are shown in Figs. 1 and 2, respectively. The spectra of the undoped hybrids ($n = \infty$) are also presented. We divide all scattering patterns corresponding to the doped samples into two regimes: i) a decreasing intensity at low q-range ($q \leqslant 0.15$ Å^{-1} and $q \leqslant 0.07$ Å^{-1}, for the U(600) and U(2000) Eu^{3+}-based hybrids, respectively) and ii) a peak located at higher q-range ($q > 0.15$ Å^{-1} for $U(600)_n$ and $q > 0.07$ Å^{-1} for $U(2000)_n$). The presence of these two regimes has already been observed in other silica–polymer hybrids and nanocomposites[31] and is characteristic of the existence of a hierarchical structure consisting of two structural levels. In the following, the structural parameters determined from SAXS results referring to the first (small) and second (large) structural level will be labeled as (1) and (2), respectively.

For the peak region at larger q, the fittings of the theoretical function $I(q)$, given by eqn. (5), to the experimental data are

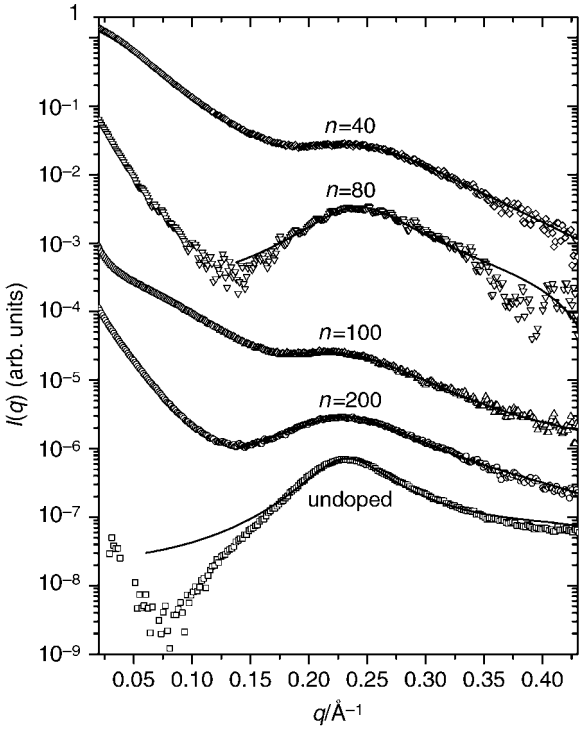

Fig. 1 Experimental SAXS curves corresponding to U(600) nanocomposites with different $n = [Eu]/[O]$ ratios. The curves are vertically displaced for clarity. Continuous lines represent the results of fitting of eqn. (5) to experimental curves.

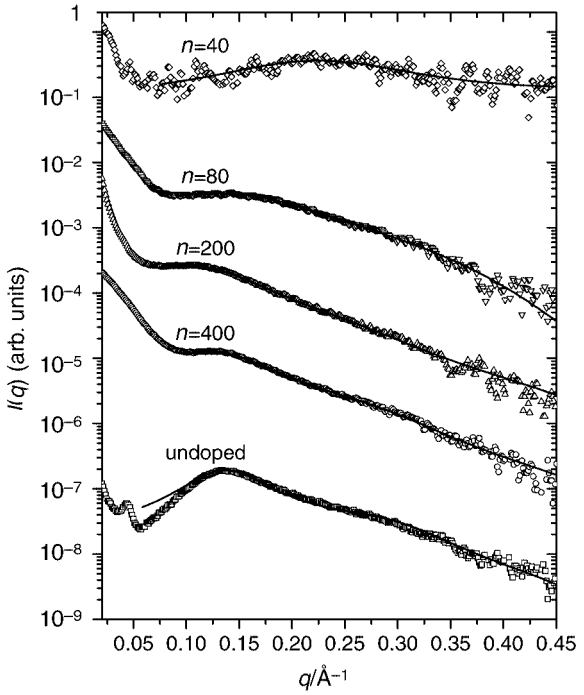

Fig. 2 Experimental SAXS curves corresponding to U(2000) nanocomposites with different n=[Eu]/[O] ratios. The curves are vertically displaced for clarity. Continuous lines represent the results of fitting of eqn. (5) to experimental curves.

displayed by the continuous lines in Figs. 1 and 2. While for the doped samples eqn. (5) agrees with the experimental observations, within $\pm 5\%$, for the non-doped hybrids the agreement is around $\pm 10\%$.

The structural parameters included in eqn. (1), (6) and (7) were determined, from the fitting procedure, for different Eu^{3+} doping concentrations. The gyration radius of the primary particles Rg_1, the interparticle distance d, the packing factor k, and the constant G, corresponding to the first structural level, are plotted in Figs. 3a and b, for $U(600)_nEu(CF_3SO_3)_3$ and $U(2000)_nEu(CF_3SO_3)_3$ hybrids, respectively.

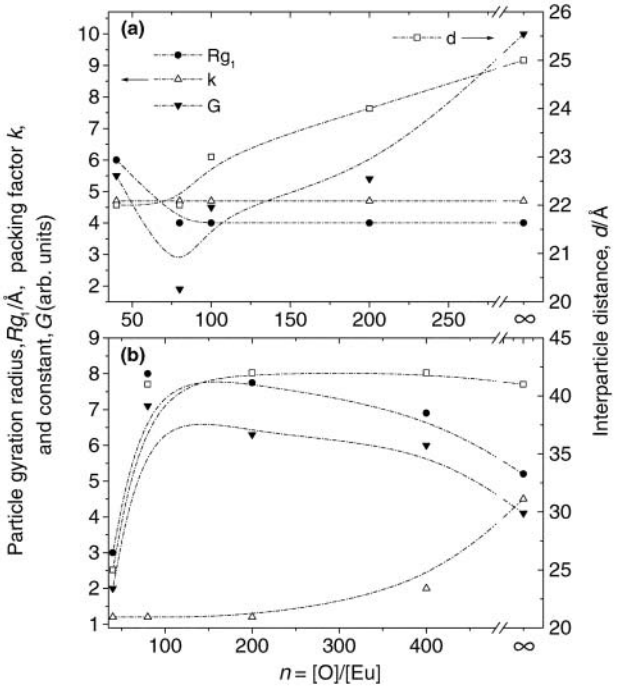

Fig. 3 Siloxane primary particle gyration radius Rg_1, interparticle distance d, packing factor k and constant G for the $U(600)_nEu(CF_3SO_3)_3$ (a) and $U(2000)_nEu(CF_3SO_3)_3$ (b) nanocomposites. Lines are drawn as guides to the eyes.

For the $U(600)_nEu(CF_3SO_3)_3$ samples two regimes can be distinguished: i) for $n \geqslant 80$, Rg_1 and k remain essentially constant at increasing europium content, whereas a decrease of d and G is observed; ii) at high europium concentration ($n=40$), an increase of the particle radius Rg_1 and the constant G occurs, the interparticle distance d and the packing factor k remaining constant.

The hybrids containing longer polymer chains, $U(2000)_nEu(CF_3SO_3)_3$, exhibit quite different behaviour: i) for $n \geqslant 80$, an increase in Rg_1 and G occurs at increasing doping level, whereas the correlation radius d remains constant. Furthermore, the presence of europium ions leads to a decrease of the packing factor k; ii) in the case of the most concentrated sample (*i.e.*, $n=40$) a strong diminution of Rg_1, d, and G is discerned.

The second structural level contributes mainly to the scattering function in the very low q range, $q \leqslant 0.15$ Å^{-1} and $q \leqslant 0.07$ Å^{-1}, for $U(600)_nEu(CF_3SO_3)_3$ and $U(2000)_nEu(CF_3SO_3)_3$, respectively. The intensity produced by the second level structure should also be described by eqn. (1), the term Rg corresponding in this case to the gyration radius of the clusters in which the siloxane primary particles are located. For all experimental scattering functions, the absence of a trend toward a constant value for decreasing q (characteristic of a Gaussian function) impedes the determination of this average size using Guinier's law. In spite of that, the maximum in the modulus of the slope in Guinier's plots, $\ln(I)$ *versus* q^2, was used to calculate a value that provides a minimum limit for the cluster sizes. A gyration radius $Rg_2 = 75 \pm 10$ Å was obtained for all samples.

Photoluminescence

The room temperature emission spectra of the $U(600)_nEu(CF_3SO_3)_3$ hybrid phosphors with $n=200$, 80 and 40 are reproduced in Fig. 4a. The photoluminescence features of the $U(2000)_nEu(CF_3SO_3)_3$ nanocomposites are similar and have been previously reported.[9,20,23–25] The narrow lines are assigned to Eu^{3+} transitions between the first excited state, $^5D_0$, and the $^7F_{0-4}$ levels of the ground septet. The $^5D_0 \rightarrow {}^7F_{5,6}$ transitions are not experimentally detected. In the case of the hybrid that incorporates the largest amount of Eu^{3+}, $U(600)_{40}Eu(CF_3SO_3)_3$, the intra-4f^6 $^5D_0 \rightarrow {}^7F_0$ transition shifts towards the blue when the excitation wavelength changes from 350 (charge transfer band) to 395 nm ($^5L_6$ level), Fig. 4b. This effect is not discerned in any other of the $U(600)_nEu(CF_3SO_3)_3$ hybrids investigated here, as Fig. 4b shows for the nanocomposite with $n=200$, and also in the di-ureasils with longer polymer chains, n between 400 and 20.[23–25]

The broad band seen in Fig. 4a has already been observed in the emission spectra of the undoped di-ureasils[9,11–13] and in those of similar hybrids.[7,8] Regarding the undoped di-ureasils, it has been recently demonstrated that this broad emission may be expressed by the convolution of a blue emission from the NH groups of the urea bridges with a purplish-blue component originated from electron–hole recombinations in the siliceous domains.[12,13] The time-resolved spectra of the Eu^{3+}-based U(600) and U(2000) di-ureasil hybrids also display two emissions with different intrinsic time scales, as Fig. 5a shows for the $U(2000)_{80}Eu(CF_3SO_3)_3$ and $U(600)_{200}Eu(CF_3SO_3)_3$ nanohybrids. We note that the incorporation of the europium salt leads to the shift towards lower energies of the two emissions mentioned above for the undoped gels. Therefore, the blue and the purplish-blue components are termed in the Eu^{3+}-containing di-ureasils as green and blue/purplish-blue, respectively. While for a delay time of 0.08 ms the hybrid spectra unambiguously exhibit these two bands, only the single green component is detected for longer delay times (5 ms), Fig. 5b. It should be stressed again that for the diamines and the

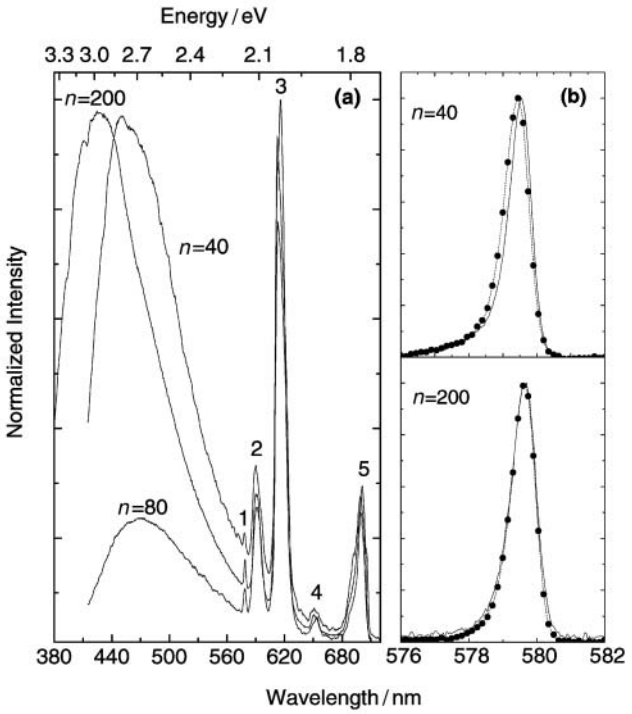

Fig. 4 (a) Emission spectra (300 K) of $U(600)_nEu(CF_3SO_3)_3$ hybrid phosphors ($n=200$, 80 and 40) excited around the maximum of the excitation spectra monitored at the $^7F_2$ level (350 nm for $n=200$ and 395 nm for the other two samples). (1), (2), (3), (4), (5): $^5D_0 \rightarrow {}^7F_{0,1,2,3,4}$. (b) The 14 K $^5D_0 \rightarrow {}^7F_0$ transition of $U(600)_nEu(CF_3SO_3)_3$ ($n=200$ and 40) excited at 350 (charge transfer band), solid line, and 395 nm ($^5L_6$), dot line with full circles.

non-hydrolyzed precursors there is no evidence of the presence of this band that clearly appears for both the undoped and the Eu^{3+}-based di-ureasils. The 14 K green and blue/purplish-blue band lifetimes in the doped xerogels are of the same order of

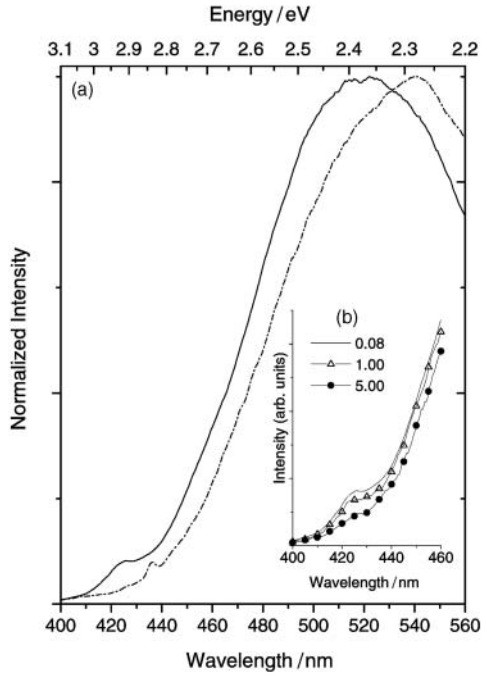

Fig. 5 (a) Time-resolved spectra (0.08 ms delay-time) for $U(2000)_{80}Eu(CF_3SO_3)_3$ (dot line) and $U(600)_{200}Eu(CF_3SO_3)_3$ (solid line), excited at 365 and 375 nm, respectively. (b) Time-resolved spectra for $U(600)_{200}Eu(CF_3SO_3)_3$ obtained at delay-times between 0.08 and 5.00 ms. All the spectra were recorded at 14 K with a 10 ms acquisition window.

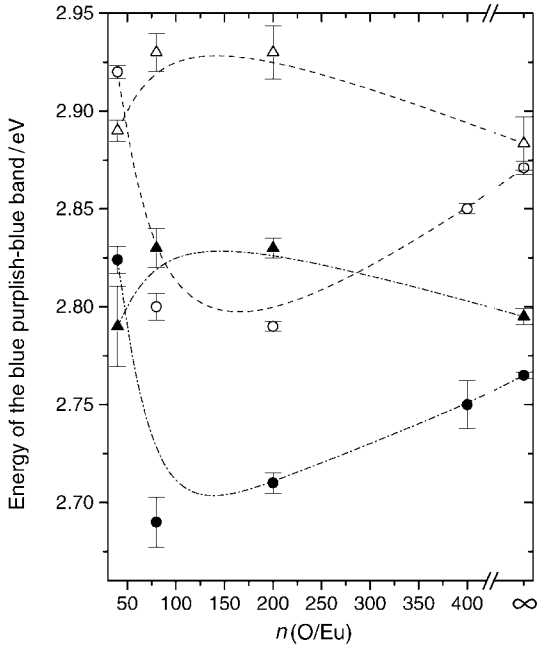

Fig. 6 Fitted energy of the siloxane-domain-connected blue/purplish-blue emission—excited at 3.14 (full circles and full triangles) and 3.40 eV (open circles and open triangles)—for the $U(600)_nEu(CF_3SO_3)_3$ and the $U(2000)_nEu(CF_3SO_3)_3$ nanocomposites, respectively. Lines are drawn as guides to the eyes.

magnitude as those found in the undoped di-ureasils (≈ 100 and ≈ 1 ms, respectively, errors within 3–5%).[13]

In silicon-based nanostructured materials the dimensional hierarchy of the backbone determines the emission energy in such a way that an increase in the siliceous network dimension results in a decrease of the corresponding energy gap.[37] Accordingly, the calculated energy of the siloxane-domain-connected blue/purplish-blue luminescence will be related next with the SAXS-determined siloxane particle radius.

For $U(600)_nEu(CF_3SO_3)_3$ the deconvolution curve-fitting procedure of the broad emission (300 K) reveals, for excitation wavelengths between 330 (3.76 eV) and 395 nm (3.14 eV), the presence of two unshaped Gaussian emissions (the green and the siloxane-domain-connected blue/purplish-blue). However, for excitation wavelengths greater than 395 nm, the room-temperature luminescence spectra were fitted just to the green component. In contrast, for $U(2000)_nEu(CF_3SO_3)_3$ nanohybrids, $400 \geqslant n \geqslant 80$, two bands could be fitted for excitation wavelengths between 330 and 420 nm.[24] The iterative least-squares curve-fitting procedure adopted is exactly the same as that reported elsewhere for the undoped di-ureasils.[11] The energy of the green component is fitted around 2.4–2.6 eV, for both di-ureasils series, whereas the values found for the blue/purplish-blue band are approximately equal to 2.5–3.0 eV, $U(2000)_nEu(CF_3SO_3)_3$, and 2.8–3.0 eV, $U(600)_nEu(CF_3SO_3)_3$. For each excitation used the variation of the emission energy of the two bands with the amount of Eu^{3+} incorporated follows approximately the same trend, as Fig. 6 shows for the blue/purplish-blue emission excited near the upper and lower limits of the excitation energy range used (3.14 and 3.40 eV).

FTIR spectroscopy

The CO stretching spectral region (νCO) is considered to be one of the most reliable tools to detect cation complexation effects in polymer electrolytes. Bonding of the ether oxygen atoms of the polymer chains to the metal ions is known to induce a redshift of the strong band at 1110 cm^{-1}, attributed to the CO stretching vibration of uncoordinated polyether

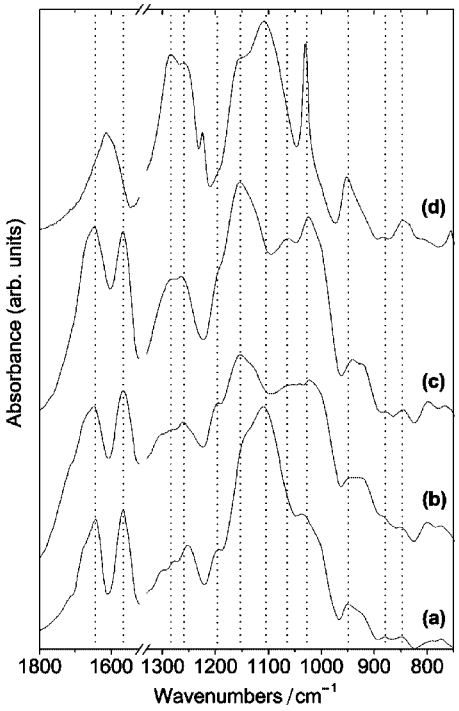

Fig. 7 Room temperature infrared spectra of $U(600)_nEu(CF_3SO_3)_3$ di-ureasils: (a) $n=\infty$, (b) $n=200$, (c) $n=60$ and (d) $n=10$.

chains.[10,38] The magnitude of the shift depends on the strength of the cation/polyether interaction. Comparison of the room temperature mid-infrared spectra of the $U(600)_nEu(CF_3SO_3)_3$ compounds (Figs. 7b–d) with the spectrum of U(600) (Fig. 7a) allows one to immediately conclude that in the salt-rich sample with $n=10$ (Fig. 7d) the νCO region is not modified by the presence of $Eu(CF_3SO_3)_3$. However, the incorporation of the guest salt into the host hybrid in xerogels with compositions $n=200$ and 60 (Figs. 7b and c, respectively) deeply affects that region. The most significant spectral change is probably the disappearance of the very intense CO stretching band due to uncoordinated polyether chains, located at 1110 and 1109 cm^{-1} in the spectra of U(600)[10] and $U(600)_{10}Eu(CF_3SO_3)_3$ (Figs. 7a and d, respectively). Also noteworthy in both spectra is the presence of a prominent feature situated at about 1154 cm^{-1} (Figs. 7b and c). In addition, the $U(600)_{200}Eu(CF_3SO_3)_3$ nanocomposite produces an intense band centred at 1022 cm^{-1} and a shoulder at higher wavenumbers (Fig. 7b). As for the spectrum of $U(600)_{60}Eu(CF_3SO_3)_3$, it displays a strong, sharp band centred at 1029 cm^{-1} and a broader one, also intense, at 1066 cm^{-1} (Fig. 7c).

Another very useful spectral region to study the interactions between the heteroatoms of the polyether chains and metal cations is that including the absorption bands originating from a mixture of skeletal stretching and CH_2 rocking vibration modes.[39,40] In this range of frequencies (1000–800 cm^{-1}) the changes observed are indicative of modifications in the local structure of the polymer backbone. Figs. 7a and d clearly show that in this region the dominating feature of the spectra of U(600) and $U(600)_{10}Eu(CF_3SO_3)_3$ is a medium intensity band located at 950 and 948 cm^{-1}, respectively, and a shoulder at 921 and 929 cm^{-1}, respectively. Both events are due to the coupled vibration of CC stretching and CH_2 rocking modes.[39,40] Two very weak bands at 879 and 850 cm^{-1}, attributed to the coupled vibration of CO stretching and CH_2 rocking modes,[39,40] are also present. In the spectra of $U(600)_{200}Eu(CF_3SO_3)_3$ (Fig. 7b) and $U(600)_{60}Eu(CF_3SO_3)_3$ (Fig. 7c) the 921 cm^{-1} shoulder is transformed into a medium intensity band at 918 cm^{-1}, whereas the 950 cm^{-1} band appears as a shoulder at 941 cm^{-1}. As for the pair of weak 879 and 850 cm^{-1} bands of U(600)[10], it may be immediately recognized from the analysis of Figs. 7b and c that their frequency is not affected by the inclusion of the guest triflate salt. While the higher frequency feature undergoes a slight upshift to 881 cm^{-1}, the other peak is shifted to approximately 847 cm^{-1}. Both bands become, however, considerably better defined in the spectra of $U(600)_{200}Eu(CF_3SO_3)_3$ (Fig. 7b) and $U(600)_{60}Eu(CF_3SO_3)_3$ (Fig. 7c).

We have stressed in earlier works that the urea Amide I and Amide II bands yield rich information, not only about the magnitude of hydrogen bonding in the undoped and Eu^{3+}-doped di-ureasils, but also about the presence (or not) of coordination of the lanthanide ions to the carbonyl oxygen atoms of the urea cross-links.[22,23,26] The Amide I mode is a highly complex vibration which involves the contribution of the C=O stretching, the C–N stretching and the C–C–N deformation vibrations.[40] We have reported that the Amide I contour of U(600) comprises three distinct components at 1715 (shoulder), 1671 (shoulder) and 1641 cm^{-1} (strong band)[10] (Fig. 7a). The latter event has been unambiguously ascribed to the formation of strong and ordered self-associated urea–urea structures which are dominant in this hybrid, because of the existence of an extremely high number of urea moieties, which is in turn a consequence of the reduced number of (OCH_2CH_2) repeat units in the organic segments.[10] The pair of shoulders has been associated with the presence of a minor number of less ordered urea–polyether structures.[10] The Amide II mode is a mixed contribution of the N–H in-plane bending, the C–N stretching and the C–C stretching vibrations.[40] In the spectrum of U(600) (Fig. 7a) the Amide II band is a single, very intense event seen at 1565 cm^{-1}. It may be readily inferred from the spectra depicted in Figs. 7b and c that the frequency and relative intensity of the urea characteristic Amide I and Amide II features of U(600) remain essentially unchanged upon addition of the guest lanthanide salt in compounds with $n=200$ and 60. Fig. 7d unequivocally demonstrates that the same spectral region is, however, deeply disturbed at high salt concentration, *i.e.*, $n=10$.

Discussion

The peak seen in the SAXS patterns of the undoped U(600) and U(2000) nanocomposites (Figs. 1 and 2) has already been observed in similar siloxane–POE hybrid materials prepared using nucleophilic catalysis.[28,29] It has been attributed to an interference effect in the X-ray scattering amplitude produced by the existence of a spatial correlation between siloxane particles embedded in the polymeric phase and located at the polymer chain ends. For the undoped U(600) and U(2000) hybrids, the good agreement found between the theoretical function, $I(q)$, of eqn. (5), and the experimental SAXS spectra in the peak region (Figs. 1 and 2) confirms the validity of the structural model already proposed for such materials.[11,28,29]

Since the photoluminescence results indicate the absence of an Eu^{3+}-rich phase (the formation of this phase would lead to a strong reduction of the $^5D_0$ lifetime, due to the non-radiative contribution of ion–ion interactions, and a significant number of new Stark components for the $^7F_{1-4}$ levels), we have assumed that the Eu^{3+} atoms are dispersed in one of the homogeneous phases of the two electron density model proposed for the undoped system. Under this assumption, the effect on SAXS intensity comes from the variation in the average electron density contrast, $\Delta\rho=\rho_p-\rho_m$, produced by the addition of Eu^{3+} atoms. In addition, the dispersed lanthanide atoms yield a constant and weak intensity background.

The strong decreasing intensity observed at low q for doped samples (Figs. 1 and 2), which is superposed to the peaked intensity at higher q, is expected for a hierarchical structure consisting of two levels (see method of SAXS analysis).

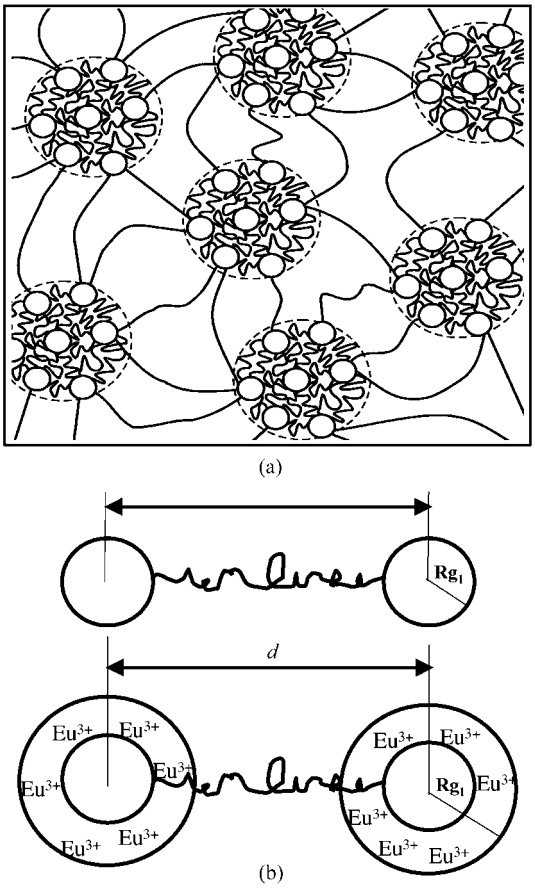

Fig. 8 (a) Schematic picture of the proposed model of a two level hierarchical structure. Small spatially correlated siloxane particles of radius Rg_1 form clusters of radius $Rg_2 > Rg_1$. Note that the polymer chains are in a folded state inside the clusters and in a nearly extended state between them. (b) Schematic model of Eu^{3+} adsorption at the siloxane–polymer interface for the di-ureasil nanocomposites.

This reveals that the incorporation of $Eu(CF_3SO_3)_3$ into the di-ureasils promotes the formation of clusters of average radius Rg_2, constituted of the spatially correlated primary siloxane particles of average radius Rg_1 separated by the average distance d. This model is illustrated in Fig. 8a and suggests that the incorporation of the triflate salt induces a partial nanophase separation of siloxane particles.

Siloxane–POE_{600} composites, $U(600)_nEu(CF_3SO_3)_3$

In hybrids containing polymer chains of low molecular weight, *i.e.*, materials of the $U(600)_nEu(CF_3SO_3)_3$ family, and at low or medium doping level ($n \geqslant 80$) the observed decrease of G with doping while the siloxane particle radius Rg_1 remains constant (Fig. 3a) can be attributed to the decrease of the electronic density contrast ($\rho_p - \rho_m$), eqn. (4). This is a consequence of filling the open space between polymeric chains by increasing the amount of Eu^{3+} ions interacting with the ether-type oxygens. This preferential interaction of europium ions with the ether oxygens of the polymer chains is confirmed by the observed decrease in the siloxane interparticle distance, d, with increasing europium content. This effect has already been reported for lithium and europium-doped hybrids[28,29,34] and has been associated to the shrinkage of the polymer structure as a consequence of an increase in the degree of cross-linking, O–Eu^{3+}–O, between polymer chains. However, this contraction of the polymer structure is small and consequently the packing factor, k, remains constant (around 4.7) over the Eu^{3+} concentration range. The observed constancy of the siloxane particle radius Rg_1 with increasing doping (from $n = 200$ to $n = 80$) is coherent with the preferential coordination of Eu^{3+} ions with the ether oxygens of the POE segments.

At $n = 40$ the observed increase of the primary particle radius Rg_1, whereas the interparticle distance d remains constant (Fig. 3a), reveals that surrounding of the siloxane particles by Eu^{3+} ions occurs. The interaction of europium ions with the oxygens of carbonyl groups of the urea bridges at the siloxane–polymer interface has already been evidenced in such materials.[22–26] As a matter of fact, the adsorption of the cations at the siloxane particles surface surrounding the carbonyl groups leads to an increase of Rg_1, without modifying the distance between particles, as illustrated in Fig. 8b. The surrounding of siloxane particles by Eu^{3+} ions also leads to the increase of the constant G (Fig. 3a), which derives both from the increase of the electronic density close to the inorganic particles and from the increase of Rg_1, eqn. (4). The coordination of cations near the siloxane particles surface at high europium contents can be explained by the lower number of "free" ether-type oxygens available to interact with europium ions in the polymeric phase.

All these interpretations are corroborated by the photoluminescence and FTIR results. The fitted energy of the siloxane-related blue/purplish-blue band remains constant between $n = 200$ and 80 and decreases for the most concentrated sample, $n = 40$, showing the expected relation between the increase of the primary siloxane particle radius and the decrease of the energy gap of the corresponding purplish-blue band, Figs. 3b and 7. Moreover, in $U(600)_{40}Eu(CF_3SO_3)_3$ a structured profile of the $^5D_0 \rightarrow {}^7F_0$ transition is clearly detected as the excitation wavelength changes from 350 to 395 nm (Figs. 4b and c). Since this line corresponds to a transition between two non-degenerate states, the blue shift detected is certainly associated with the presence of Eu^{3+} sites subject to distinct effective local fields. Therefore, this result is a strong indication that in the case of the U(600) hybrid host the incorporation of larger amounts of Eu^{3+} ions induces two different local site coordinations, in contrast to the $U(2000)_nEu(CF_3SO_3)_3$ di-ureasils ($400 \geqslant n \geqslant 20$) where there is no evidence of distinct Eu^{3+} local coordination sites.[23–25]

The exclusive role of the ether oxygen atoms of the polymer segments of U(600) in the complexation of the lanthanide ions and the non-participation of the carbonyl oxygen atoms of the cross-links in this process for materials with compositions greater than 40 (in the present study, $n = 200$ and 60) is in full agreement with several pieces of evidence found in the infrared spectra discussed previously: (1) the absence in both cases of the 1100 cm^{-1} absorption band, characteristic of uncomplexed polyether moieties, and the presence of a strong component around 1066–1069 cm^{-1}, assigned to coordinated polymer segments; (2) the contour of the Amide I and Amide II envelopes, which remains unchanged after the addition of salt to U(600), clearly indicating that the extent and strength of hydrogen bonding throughout the hybrid host material remains essentially unaffected in the presence of $Eu(CF_3SO_3)_3$ within this range of salt concentration. The latter experimental observation also implies that in both samples the cations are unable to disrupt the strong and ordered hydrogen-bonded network of U(600) involving the urea N–H groups and the oxygen atoms of the urea carbonyl groups and those of the polyether chains.[10] As bonding to the urea linkages is not permitted, it becomes compulsory for the Eu^{3+} ions to interact with the ether oxygens of the polymer chains. Similar findings have been also discerned in the FTIR spectra of U(600)-based di-ureasils doped with $Eu(ClO_4)_3$ at compositions $n = 232$ and 62, thus very close to the ones investigated here.[26]

The inclusion of $U(600)_{10}Eu(CF_3SO_3)_3$ in the present study has enabled us to clearly illustrate that the opposite situation occurs at high salt content. In this particular case, no spectral evidence of the involvement of the polymer chains in the complexation of the lanthanide ions has been found. On the

contrary, we have reported the presence of a series of characteristic spectral features that are consistent with bonding of the cations to the urea carbonyl oxygen atoms. These results suggest that at high $Eu(CF_3SO_3)_3$ concentration the hydrogen-bonded urea–urea structures of U(600) are easily destroyed, rendering the coordinating urea groups completely free. Under such conditions the carbonyl oxygen atoms ensure the coordination of the cations, leaving the polymer chains completely excluded from this process.

Siloxane–POE_{2000} composites, $U(2000)_nEu(CF_3SO_3)_3$

The behaviour as a function of doping of the hybrids containing polymer chains of higher molecular weight, $U(2000)_nEu(CF_3SO_3)_3$, is exactly the opposite of that observed for the $U(600)_nEu(CF_3SO_3)_3$ ones.

At low and medium doping levels ($n \geqslant 80$) the preferential coordination sites for the cations are the oxygens of carbonyl groups located in the urea bridges at the siloxane–polymer interface (Fig. 8b). This is supported by the observed increase of the primary particle radius Rg_1 at increasing doping level up to a composition of $n=80$, whereas the interparticle distance d remains constant (Fig. 3b). This is also confirmed by the observed increase of G in the same doping range (Fig. 3b), as a consequence of the increase of both the electronic density contrast between siloxane particles and the POE matrix and of the increase of the particle radius Rg_1. Furthermore, this interpretation is also coherent with the strong diminution of the value of the packing factor k upon doping (Fig. 3b), which is very likely due to the increasing electrostatic repulsion between siloxane particles surrounded by Eu^{3+} ions. Therefore, all these results confirm that, at low and medium doping level, the cations interact preferentially with the carbonyl oxygen atoms in hybrids containing long polymer chains, as already suggested by mid-infrared[22,23] and photoluminescence[23–25] spectroscopic studies carried out previously.

Different behaviour is observed at high Eu^{3+} concentration (*i.e.*, $n=40$): the decreasing trend of the particle radius Rg_1 (Fig. 3b) reveals that polycondensation reactions between silicon species located at chain ends are inhibited during gelation. The hypothesis of this being induced by the increase of polymer chains rigidity due to their interaction with Eu^{3+} ions (*e.g.* coordination of the cations with the ether oxygens of POE) is completely discarded both by the photoluminescence[23–25] and FTIR[22,23] data and also by the smooth variation of the glass transition temperature.[22] In fact, when the emission spectra of the U(2000)-based hybrids are compared as the Eu^{3+} amount increases from $n=400$ to 40 no trace of a distinct Eu^{3+} local environment could be discerned. In addition, for $U(2000)_{40}Eu(CF_3SO_3)_3$ the energy of the $^5D_0 \rightarrow {}^7F_0$ line (with respect to the value reported for the free ion case) was nicely predicted considering a Eu^{3+}-first coordination shell involving two carbonyl oxygens, four oxygen atoms from the SO_3 groups, and five water molecules.[25]

All the results presented above indicate that the diminution of the particle radius Rg_1—and as a consequence of d (Fig. 3b)—observed in the $U(2000)_{40}Eu(CF_3SO_3)_3$ hybrid may be related to the decrease of the number of carbonyl groups from the urea cross-linkages available for coordination per each Eu^{3+} incorporated. This number decreases from 4 to 2 as the Eu^{3+} concentration increases from $n=80$ to 40.[24,25] Therefore, for such latter europium content, all of the carbonyl-type oxygens present in the hybrid interact with an Eu^{3+} cation. Normally, in this case, the two carbonyl oxygen atoms interacting with each Eu^{3+} ion should be located in two different polymer chains, thus leading to the formation of –C=O–Eu^{3+}–O=C– cross-links between the two chains, at the inorganic–POE interface. This effect inhibits the polycondensation reactions due to the reduced mobility in the sol of the entities constituted of double chains and the silicon species located at their ends. Since the cross-links are situated near the inorganic phase–polymer interface, this process does not affect the mobility of each POE chain. The resulting diminution in siloxane particle size is responsible for the diminution of the constant G, Fig. 3b and eqn. (4). Again we found the expected trend between the increase (decrease) of the primary siloxane particle radius and the decrease (increase) of the energy gap of the corresponding blue/purplish-blue band, Figs. 3b and 7.

Conclusions

The local structure of sol–gel derived Eu^{3+}-based nanohybrids, in which a siliceous skeleton is grafted onto poly(oxyethylene) chains of variable length through urea bridges, was modelled using the results of a number of experimental techniques.

The incorporation of europium ions into the nanohybrid hosts promotes the formation of a two-level structure in which the primary level is composed of rather close-packed siloxane nanoparticles. Clusters of these particles form the second level. Considering the covalent nature of the siloxane particles–polymer chains bonds, we conclude that polymer chains in a strongly folded state connect the siloxane particles inside each cluster, resulting in a strong spatial correlation between particles. In contrast, polymer chains in a nearly extended (unfolded) conformation link siloxane particles located in different clusters (Fig. 8a).

The nature of the Eu^{3+} first coordination shell varies both with the salt concentration and with the number of oxyethylene repeat units. In di-ureasils containing long organic segments, $U(2000)_nEu(CF_3SO_3)_3$, and at compositions n between 400 and 40, the Eu^{3+} ions interact mainly with the carbonyl-type oxygens of the urea cross-links located at the organic/inorganic interface. In contrast, in the $U(600)_nEu(CF_3SO_3)_3$ di-ureasils, $n \geqslant 60$, as the Eu^{3+} ions are unable to disrupt the strong and ordered hydrogen-bonded urea–urea structures the preferential coordination sites are the ether-type oxygens of the polymer chains. However, for high-salt concentration hybrids, $n \leqslant 40$, besides the coordination to the polymer ether oxygens a distinct cation local site environment involving the interaction with the urea carbonyl oxygens atoms at the siloxane–POE interface is detected. For $n=10$ the hydrogen-bonded urea–urea structures of the U(600) network are probably destroyed by the larger amount of salt present, and, therefore, the carbonyl oxygens of the urea cross-links are the only active coordinating groups. We should remember that in these hybrids only at compositions lower than approximately 4 there is one urea group per each incorporated Eu^{3+} ion. This ability to tune the Eu^{3+} coordination between the carbonyl oxygens of the urea groups and the ether oxygen atoms of the poly(oxyethylene) chains—controlling both the salt concentration and the polymer molecular weight—illustrates one of the most interesting features of these materials and opens new prospects into their potential fields of application.

Acknowledgements

The authors thank the collaboration of LNLS staff and A. P. Passos de Almeida during SAXS and FTIR measurements, respectively. The financial support from FCT, (PRAXIS/P/CTM/13175/98, BD/18404/98) and ICCTI, from Portugal, and FAPESP and CAPES, from Brazil, is gratefully acknowledged.

References

1 (*a*) C. J. Brinker and G. W. Scherrer, *Sol–Gel Science, The Physics and Chemistry of Sol–Gel Processing*, Academic Press, San Diego, CA, 1990; (*b*) H. Schmidt, in *Chemical Processing of Advanced Materials*, ed. L. L. Hench and J. K. West, Wiley, New York, 1992, ch. 64

2 *Hybrid Organic–Inorganic Materials*, ed. L. L. Klein and C. Sanchez, Special issue of *J. Sol–Gel Sci. Technol.*, 1995, **5**.
3 (*a*) B. Novak, *Adv. Mater.*, 1993, **5**, 422; (*b*) U. Schubert, N. Hüsing and A. Lorenz, *Chem. Mater.*, 1995, **7**, 2010.
4 (*a*) J. Wen and G. L. Wilkes, *Chem. Mater.*, 1996, **8**, 1667; (*b*) P. Judeinstein and C. Sanchez, *J. Mater. Chem.*, 1996, **6**, 511; (*c*) C. Sanchez, F. Ribot and B. Lebeau, *J. Mater. Chem.*, 1999, **9**, 35.
5 (*a*) *Sol–Gel Optics II*, ed. J. D. Mackenzie, *Proc. SPIE*, Bellingham, Washington, 1992, vol. 1758; (*b*) *Sol–Gel Optics III*, ed. J. D. Mackenzie, *Proc. SPIE*, Bellingham, Washington, 1994, vol. 2288.
6 (*a*) E. J. A. Pope, *J. Sol–Gel Sci. Technol.*, 1994, **2**, 717; (*b*) H. Law, T. Tou and S. Ng, *Appl. Opt.*, 1998, **37**, 5694.
7 W. H. Green, K. P. Le, J. Grey, T. T. Au and M. J. Sailor, *Science*, 1997, **276**, 1826.
8 (*a*) V. Bekiari and P. Lianos, *Chem. Mater.*, 1998, **10**, 3777; (*b*) V. Bekiari and P. Lianos, *Langmuir*, 1998, **14**, 3459.
9 L. D. Carlos, V. de Zea Bermudez, M. C. Duarte, M. M. Silva, C. J. Silva, M. J. Smith, M. Assunção and L. Alcácer, in *Physics and Chemistry of Luminescent Materials VI*, ed. C. Ronda and T. Welker, Electrochemical Society, San Francisco, 1998, vol. 97–29, p. 352.
10 V. de Zea Bermudez, L. D. Carlos and L. Alcácer, *Chem. Mater.*, 1999, **11**, 569.
11 L. D. Carlos, V. de Zea Bermudez, R. A. Sá Ferreira, L. Marques and M. Assunção, *Chem. Mater.*, 1999, **11**, 581.
12 L. D. Carlos, R. A. Sá Ferreira, V. de Zea Bermudez, I. Orion and J. Rocha, *J. Lumin.*, 2000, **87–89**, 702.
13 L. D. Carlos, R. A. Sá Ferreira, V. de Zea Bermudez and S. J. L. Ribeiro, *Adv. Funct. Mater.*, 2001, **2**, 111.
14 G. F. de Sá, O. L. Malta, C. M. Donegá, A. M. Simas, R. L. Longo, P. A. Santa-Cruz and E. F. da Silva, *Coord. Chem. Rev.*, 2000, **196**, 165.
15 L. R. Matthews and E. T. Knobbe, *Chem. Mater.*, 1993, **5**, 1697.
16 V. C. Costa, M. J. Lochhead and K. L. Bray, *Chem. Mater.*, 1996, **8**, 783.
17 (*a*) A. C. Franville, D. Zambon, R. Mahiou, S. Chou, Y. Troin and J. C. Cousseins, *J. Alloys Compd.*, 1998, **275–277**, 831; (*b*) A. C. Franville, D. Zambon and R. Mahiou, *Chem. Mater.*, 2000, **12**, 428.
18 (*a*) H.-H. Li, S. Inoue, D. Ueda, K.-I. Machida and G.-Y. Adachi, *Electron. Solid State Lett.*, 1999, **2**, 354; (*b*) H.-H. Li, S. Inoue, K.-I. Machida and G.-Y. Adachi, *Chem. Mater.*, 1999, **11**, 3171.
19 (*a*) M. Armand, C. J. Poinsignon, J.-Y. Sanchez and V. de Zea Bermudez, *US Pat.*, 1994, 5283310; (*b*) V. de Zea Bermudez, D. Baril, J.-Y. Sanchez, M. Armand and C. J. Poinsignon, in *Optical Materials Technology for Energy Efficiency and Solar Conversion XI: Chromogenics for Smart Windows*, ed. A. Hugot-Le Golf, C.-G. Granqvist and C. M. Lampert, *Proc. SPIE*, Bellingham, Washington, 1992, vol. 1728, p. 180; (*c*) V. de Zea Bermudez, C. J. Poinsignon and M. Armand, *J. Mater. Chem.*, 1997, **7**, 1677.
20 V. de Zea Bermudez, L. D. Carlos, M. C. Duarte, M. M. Silva, C. J. Silva, M. J. Smith, M. Assunção and L. Alcácer, *J. Alloys Compd.*, 1998, **275–277**, 21.
21 S. J. L. Ribeiro, K. Dahmouche, C. A. Ribeiro, C. V. Santilli and S. H. Pulcinelli, *J. Sol–Gel Sci. Technol.*, 1998, **13**, 427.
22 M. M. Silva, V. de Zea Bermudez, L. D. Carlos, A. P. Passos de Almeida and M. J. Smith, *J. Mater. Chem.*, 1999, **9**, 1735.
23 L. D. Carlos, V. de Zea Bermudez and R. A. Sá Ferreira, *J. Non-Cryst. Solids*, 1999, **247**, 203.
24 L. D. Carlos, R. A. Sá Ferreira, V. de Zea Bermudez, C. Molina, L. A. Bueno and S. J. L. Ribeiro, *Phys. Rev. B*, 1999, **60**, 10042.
25 L. D. Carlos, Y. Messaddeq, H. F. Brito, R. A. Sá Ferreira, V. de Zea Bermudez and S. J. L. Ribeiro, *Adv. Mater.*, 2000, **12**, 594.
26 V. de Zea Bermudez, R. A. Sá Ferreira, L. D. Carlos, C. Molina, K. Dahmouche and S. J. L. Ribeiro, *J. Phys. Chem. B*, 2001, **105**, 3378.
27 V. Bekiari, P. Lianos and P. Judeinstein, *Chem. Phys. Lett.*, 1999, **307**, 310.
28 K. Dahmouche, C. V. Santilli, S. H. Pulcinelli and A. F. Craievich, *J. Phys. Chem. B*, 1999, **103**, 4937.
29 K. Dahmouche, C. V. Santilli, M. da Silva, C. A. Ribeiro, S. H. Pulcinelli and A. F. Craievich, *J. Non-Cryst. Solids*, 1999, **247**, 108.
30 D. E. Rodrigues, A. B. Brennan, C. Betrabet, B. Wang and G. L. Wilkes, *Chem. Mater.*, 1992, **4**, 1437.
31 G. Beaucage, T. A. Ulibarri, E. P. Black and D. W. Schaefer, in *Hybrid Organic–Inorganic Composites*, ed. J. E. Mark, C. Y.-C. Lee and P. A. Bianconi, *Am. Chem. Soc. Symp. Proc.*, ACS, Washington, 1995, vol. 585, p. 97.
32 I. Krakovsky, H. Urakawa, K. Kajiwara and S. Kohjiya, *J. Non. Cryst. Solids*, 1998, **231**, 31.
33 N. Maene, B. N. Nair, P. D'Hooge, S. I. Nakao and K. Keizer, *J. Sol–Gel Sci. Technol.*, 1998, **12**, 117.
34 C. Molina, S. J. L. Ribeiro, K. Dahmouche, C. V. Santilli and A. F. Craievich, *J. Sol–Gel Sci. Technol.*, 2000, **19**, 615.
35 *Small-Angle Scattering of X-rays*, ed. A. Guinier and G. Fournet, John Wiley and Sons, New York, 1955, p. 55.
36 *Small Angle X-ray Scattering*, ed. O. Glatter and O. Kratky, Academic Press, New York, 1982.
37 (*a*) T. Takagahara and K. Takeda, *Phys. Rev. B*, 1992, **46**, 15578; (*b*) G. Allan, C. Delerue and M. Lannoo, *Phys. Rev. B*, 1993, **48**, 7951; (*c*) Y. Kanemitsu, K. Susuki, S. Kyushin and H. Matsumoto, *Phys. Rev. B*, 1995, **51**, 13103; (*d*) A. O. Konstantinov, A. Henry, C. I. Harris and E. Janzén, *Appl. Phys. Lett.*, 1995, **66**, 2250.
38 (*a*) H. Matsuura and T. Miyazawa, *J. Polym. Sci. A*, 1969, **7**(2), 1735; (*b*) K. Machida and T. Miyazawa, *Spectrochim. Acta*, 1964, **20**, 1865.
39 H. Matsuura, T. Miyazawa and K. Machida, *Spectrochim. Acta*, 1973, **29A**, 771.
40 T. Miyazawa, T. Shimanouchi and S.-I. Mizushima, *J. Chem. Phys.*, 1956, **24**, 408.